Article

Investigation on the Corrosion Resistance of 3003 Aluminum Alloy in Acidic Salt Spray under Different Processing States

Qiang Lu [1], Yuchao Zhao [1], Qudong Wang [1,*] and Dezhi Li [2]

[1] National Engineering Research Center of Light Alloy Net Forming, State Key Laboratory of Metal Matrix Composites, School of Materials Science and Engineering, Shanghai Jiao Tong University, Shanghai 200240, China; luqiang951127@sjtu.edu.cn (Q.L.); zhaoyuchao@sjtu.edu.cn (Y.Z.)

[2] Warwick Manufacturing Group, University of Warwick, Coventry CV4 7AL, UK; dezhi.li@warwick.ac.uk

[*] Correspondence: wangqudong@sjtu.edu.cn

Abstract: 3003 aluminum alloy exhibits commendable corrosion resistance, ease of processing, and good formability, rendering it extensively utilized across many industrial sectors. In this study, the corrosion behavior of 3003 aluminum alloy in a homogenized state and after hot extrusion deformation in an acidic salt spray environment for different times was studied. The microstructure of the 3003 aluminum alloy in the homogenized state and after hot extrusion was characterized using scanning electron microscopy (SEM), optical microscope (OM), laser scanning confocal microscope (LSCM) etc., while electrochemical methods were employed to study the difference in corrosion resistance between these two states. The results show that corrosion pits on the surface of the homogenized 3003 aluminum alloy increase with time, and corrosion extends along the second phase arrangement, while the hot extruded 3003 aluminum alloy mainly exhibits corrosion pit extension. The grain size of the homogenized 3003 aluminum alloy is larger than that of the hot extruded state, and the second phase is distributed in a reticular pattern. Hot extrusion deformation ensures not only a uniform distribution of the second phase in the 3003 aluminum alloy but also a reduced grain size, an increased grain boundary density, a heightened electrochemical activity in acidic environments, and an augmented pitting density. Compared with the homogenized 3003 aluminum alloy, the pitting density, maximum pitting depth, and weight loss of the hot extruded state are increased.

Keywords: 3003 alloy; homogenization; hot extrusion; acid salt spray; pitting corrosion; microstructure; electrochemical tests

1. Introduction

Aluminum and its alloys exhibit favorable mechanical properties, lightweight characteristics, and corrosion resistance. These materials have increasingly used across various engineering fields in recent years [1–3]. The Al-Mn alloy, a non-heat treatment-strengthened aluminum alloy, distinguishes itself with good plasticity, with exceptional processing and welding capabilities. It exhibits higher strength compared to pure aluminum while retaining corrosion resistance comparable to that of pure aluminum [4,5]. In addition, as the main alloying element, the strength of the alloy increases with the increase of Mn content. Mn can also form an Al_6Mn phase with Al, and impurity Fe can dissolve in Al_6Mn to form $Al_6(MnFe)$ compounds [6,7]. 3003 aluminum alloy is one of the most common aluminum manganese alloys, which is widely used in building construction, food packaging, automotive parts, and air conditioning radiators due to its good formability, corrosion resistance, and welding performance [8–10].

The corrosion resistance of aluminum alloys is affected by a number of factors, and fine-tuning the composition of the alloy may be considered to improve corrosion resistance [11]. For example, the addition of Cu or Zr may help improve the corrosion resistance of aluminum alloys [12,13]. The introduction of corrosion inhibitors, such as organic corrosion inhibitors, forms a protective film that slows the corrosion process [14]. In addition,

the shape, size, and distribution of the second phase also have a certain impact on the corrosion performance of aluminum alloys. Clustered second phases make aluminum alloys more susceptible to localized corrosion, and deformation or the introduction of dispersed particles is considered to be an effective way to improve the second phase in aluminum alloys [15,16]. In practical applications, the 3003 alloy is primarily employed after plastic deformation. It can undergo different processes, such as rolling, extrusion, stretching, and other forming methods, to manufacture products of various shapes [17]. In many of these applications, the 3003 aluminum alloy is either continuously or temporarily exposed to corrosive environments. Generally speaking, when aluminum and its alloys are exposed to the atmosphere, a dense oxide layer (Al_2O_3) can be formed on the surface, so aluminum has high corrosion resistance [18–20]. The oxide film is in a continuous state of breakdown and repair. In noncorrosive environments, it can be immediately repaired [21–23]. However, in the presence of solutions containing corrosive ions, especially chlorides, these anions entering the metal surface will prevent repair [24,25]. In addition, temperature and pH value in the external environment can also affect the decomposition and repair of the oxide film on the surface of aluminum alloys. Currently, most studies on the corrosion resistance of 3003 aluminum alloy are conducted separately in cast or deformed forms. Chen et al. [26] investigated the corrosion and electrochemical behavior of 3003 aluminum alloy plates in ethylene glycol–water solution at different temperatures. The results indicate that the increase in temperature accelerates the dissolution of anode aluminum and the reduction of cathode oxygen. Liu et al. [27] found that the passivation film formed on 3003 aluminum alloy cast rod is the most stable in a chlorine free solution, while the passivation film formed in a chlorine containing solution is the least stable. The film formed in air falls between the two. Yin et al. [28] found that homogenization treatment can change the quantity, distribution and morphology of the second phase in 3003 aluminum alloy, thus affecting the corrosion resistance.

Due to the wide application of 3003 aluminum alloy, there are many studies on the corrosion behavior of 3003 aluminum alloy in different environments. Liu et al. [29] studied the passivation and pitting behavior of 3003 aluminum alloy round bar in aqueous ethylene glycol solution using various electrochemical measurements. Statistical evaluation of pitting susceptibility of 3003 aluminum sheets in a saltwater environment using pitting coefficient criteria was used by Paredes-Dugarte et al. [30]. Sun et al. [31] studied the short-term and long-term corrosion behavior of 3003 aluminum alloy in saturated Na_2SO_4 solutions at different temperatures. Additionally, corrosion resistance research on aluminum alloys can be conducted using a salt spray test. These real-world challenging conditions can be emulated through a salt spray test, offering an improved assessment of material corrosion resistance [32,33].

In this study, we prepared homogenized 3003 aluminum alloy cast rods and deformed the rods by hot extrusion. A comparative analysis was conducted on the corrosion resistance, microstructure, corrosion morphology, and electrochemical test results of 3003 aluminum alloy under acidic salt spray corrosion after different times in both the homogenized and hot extrusion states. The research results can provide guidance for the practical engineering application and corrosion protection of 3003 aluminum alloy in acidic environments such as marine engineering and chemical industry.

2. Materials and Methods

The present study was carried out using commercial 3003 aluminum alloy. The 3003 aluminum alloy was homogenized and hot extruded, and acidic salt spray corrosion tests, microstructure characterization, and electrochemical tests were performed on the 3003 aluminum alloy in both processed states to study its corrosion behavior.

2.1. Materials

The 3003 alloy round bar used in the experiment was provided by Henan Runze Light Alloy Technology Co., Ltd. (Pingdingshan City, China), and its composition is shown

in Table 1. The composition of the 3003 aluminum alloy was determined by inductively coupled plasma-optical emission spectrometry (ICP-OES).

Table 1. Chemical composition of the 3003 alloy, wt%.

Element	Si	Fe	Cu	Mn	Zn	Al
%	0.12	0.36	0.15	1.08	0.10	Balance

2.2. Preparation of Homogenized and Hot Extruded 3003 Aluminum Alloy

The homogenization process of the 3003 aluminum alloy casting rod involves putting the rod in a furnace of 595 ± 5 °C for a duration of 12 h, followed by air cooling to 250 °C and then rapid cooling with strong wind until reaching room temperature. A cylinder measuring 59 mm in diameter and 30 mm in height was obtained from the homogenized aluminum rod for subsequent hot extrusion deformation. Prior to hot extrusion, the 3003 aluminum alloy underwent preheating at a temperature of 540 °C for a period of 0.5 h using a box furnace, with the mold temperature set at 400 °C and an extrusion ratio of 55:1. After extrusion, it transformed into a strip with a cross-section dimension of 25 mm × 2 mm.

2.3. Acid Salt Spray Test

Specimens were cut to 30 × 25 × 2 mm for the acid salt spray corrosion test. The corrosion tests were carried out according to ASTM G85-2011 standard [34]. The exposure zone of the acetic acid–salt spray fog chamber was maintained at 35 ± 2 °C, and the temperature in saturator tower was 47 °C. The salt solution was 50 g/L NaCl, and the pH was adjusted to 3.0–3.1 with acetic acid. The block-shaped sample was tilted and placed in a V-shaped groove at a 30° angle to the vertical direction. The samples for salt spray testing were recovered at different time intervals, up to a maximum of 4 days. Two parallel samples were set for each group. The corroded samples were mechanically cleaned under running water to remove salt deposits from their surfaces, then dried and weighed using an analytical balance to obtain weight loss.

2.4. Electrochemical Measurements

The electrochemical measurements were carried out on DH3000 electrochemical workstation using the conventional three-electrode system, with 3003 aluminum alloy as the working electrode, saturated calomel electrode (SCE) as the reference electrode (preserved in saturated KCl solution before), and a platinum plate as the counter electrode. The test was conducted in 50 g/L sodium chloride (NaCl) acetic acid solution (with pH = 3.0–3.1). The samples were immersed in electrolyte solution for at least 30 min, and then the open circuit potential (OCP) was measured until it became stable. All the other electrochemical tests were conducted based on a stable OCP. Repeatability was tested by measuring at least three specimens.

Electrochemical impedance spectroscopy (EIS) was tested to evaluate the corrosion behavior of the alloys in a frequency range from 100 KHz to 10 mHz. The polarization curves of the dynamic potential were measured to characterize the corrosion behavior of 3003 alloy in both homogenized and hot extruded states. The potentiodynamic polarization tests were carried out in a potential range of $-0.6{\sim}0.4$ V vs. OCP with a scanning rate of 1.0 mV s^{-1}.

2.5. Microstructure Examination

X-ray diffraction (XRD) measurements were performed on 3003 aluminum alloy using a D8 DaVinci X-ray diffractometer with 0.02° step size, scan range 10–90°, Cu Kα at 40 kV and 40 mA. An optical microscope (OM, LEICA DM 4000, Wetzlar, Germany) was employed to examine the metallographic structure of the 3003 aluminum alloy in both the homogenized and hot extruded states. Field emission scanning electron microscopy (SEM, Nova Nano SEM 230, Waltham, MA, USA) equipped with energy dispersive X-ray

spectroscopy (EDS) was used to characterize the corrosion morphology and corrosion product composition of the 3003 aluminum alloy. The three-dimensional morphology of the corrosion pits was characterized by laser scanning confocal microscope (LSCM, Keyence VK-X3000, Osaka, Japan).
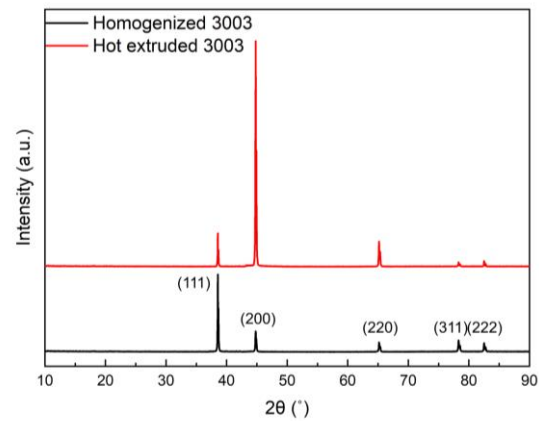
3. Results

3.1. Microstructure

The microstructure of 3003 aluminum alloy in the homogenized state and after hot extrusion is shown in Figure 1. After homogenization treatment, the grain size of the 3003 aluminum alloy became relatively uniform. When the 3003 aluminum alloy was hot extruded, the grain size was significantly reduced compared to the homogenized structure because the alloy underwent heavy deformation and recrystallization during the hot extrusion process. As shown in Figure 1c, the average grain size of 3003 aluminum alloy in a homogeneous state was about 104.5 μm, and that of 3003 aluminum alloy in hot extruded state was about 54.5 μm.
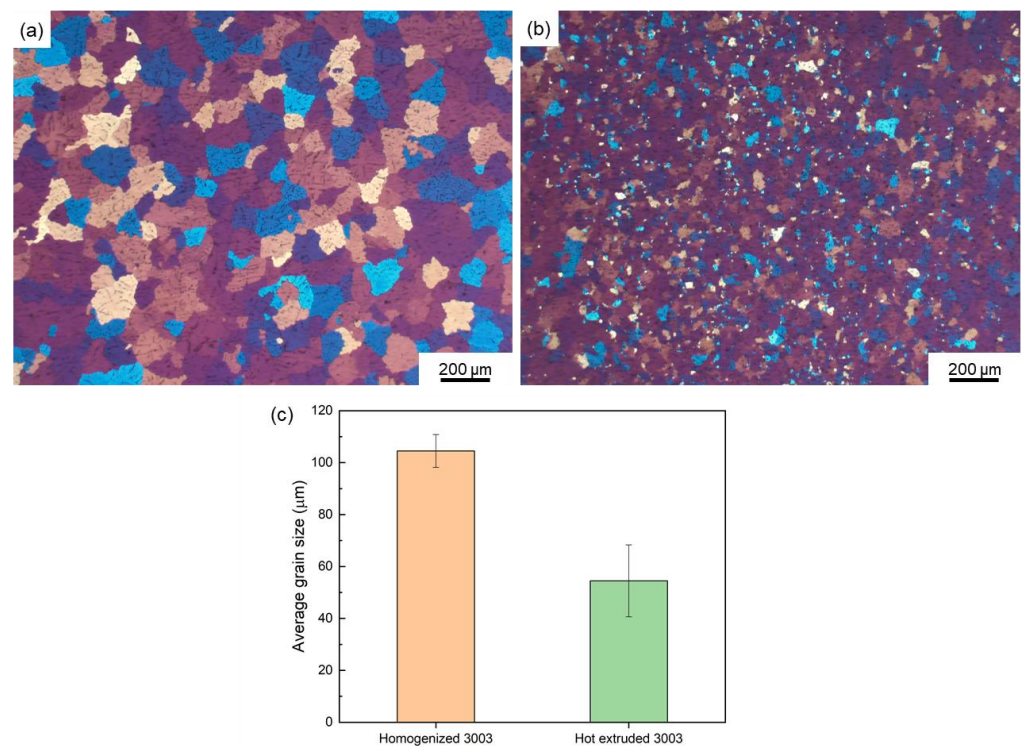
Figure 1. The microstructure of 3003 aluminum alloy under different processing states, (**a**) homogenized, (**b**) hot extruded, (**c**) comparison of average grain size of 3003 aluminum alloy in homogenized and hot extruded.

Figure 2 shows the XRD patterns of the 3003 aluminum alloy in both homogenized and hot extruded states. Due to the low content of alloying elements and the small and numerous second phases, the 3003 alloy in both processing states only shows the peak of α-Al. At the same time, it can be observed that after hot extrusion, there is a clear preferred orientation in the 3003 alloy, with the strongest diffraction peak intensity on the (200) plane. On the contrary, the strongest diffraction peak in the homogenized state is (111). Therefore, after hot extrusion, the grains of 3003 aluminum alloy deformed and developed a significant (200) preferred orientation.

Figure 2. X-ray diffraction spectrums of 3003 aluminum alloy under different processing states.

The second phase distribution of the 3003 aluminum alloy in a homogenized state and after hot extrusion is shown in Figure 3. The homogenization treatment can diffuse the alloy elements in the 3003 aluminum alloy, so that the second phase is evenly distributed within the grains, reducing the possibility of local concentration differences in the alloy and help to improve the uniformity and stability of the alloy. In Figure 3a, the second phase of the homogenized 3003 aluminum alloy is mainly distributed in a continuous reticular pattern. When the alloy was in the cast state, the second phase precipitated mainly along the grain boundaries. After the homogenization treatment, the grains grew, the second phase was partially dissolved in the matrix, and most of the second phase still maintained a reticular distribution. After hot extrusion, as shown in Figure 3b, the second phase of the 3003 aluminum alloy was no longer arranged in a reticular pattern but was evenly arranged along the extrusion direction. In both homogenized and hot extruded states, the shape of the second phase included strips and granules. The average size of the second phase in the homogenized 3003 was slightly smaller than in the hot extruded state, about 2.1 µm for the homogenized 3003, and 2.54 µm for the hot extruded 3003. The EDS results of the second phase of 3003 aluminum alloy in different states are shown in Table 2. In both states, the second phase was mainly Al-Mn-Fe, with a small amount of Al-Mn-Fe-Si. Mn, the main alloying element in the 3003 aluminum alloy can form an Al_6Mn phase with Al, while Fe can form a solid solution in the Al_6Mn phase to form an Al_6 (MnFe) compound, thereby reducing the solubility of Mn in Al. Si can also form Al-Mn-Fe-Si. Fe and Si can accelerate the decomposition of Mn from the supersaturated solid solution during thermal deformation.

**Table 2.** EDS results of the different second phases in Figure 3 (wt%).

Processing Status	Points	Mn	Fe	Si	Al
Homogenized	A	11.84	7.20		80.96
	B	11.29	7.39	3.49	77.83
	C	9.18	5.90		84.92
	Standard Deviation	1.40	0.81		3.55
Hot extruded	D	11.92	7.82		80.25
	E	8.07	6.80		85.13
	F	10.11	7.90		81.99
	Standard Deviation	1.93	0.61		2.47
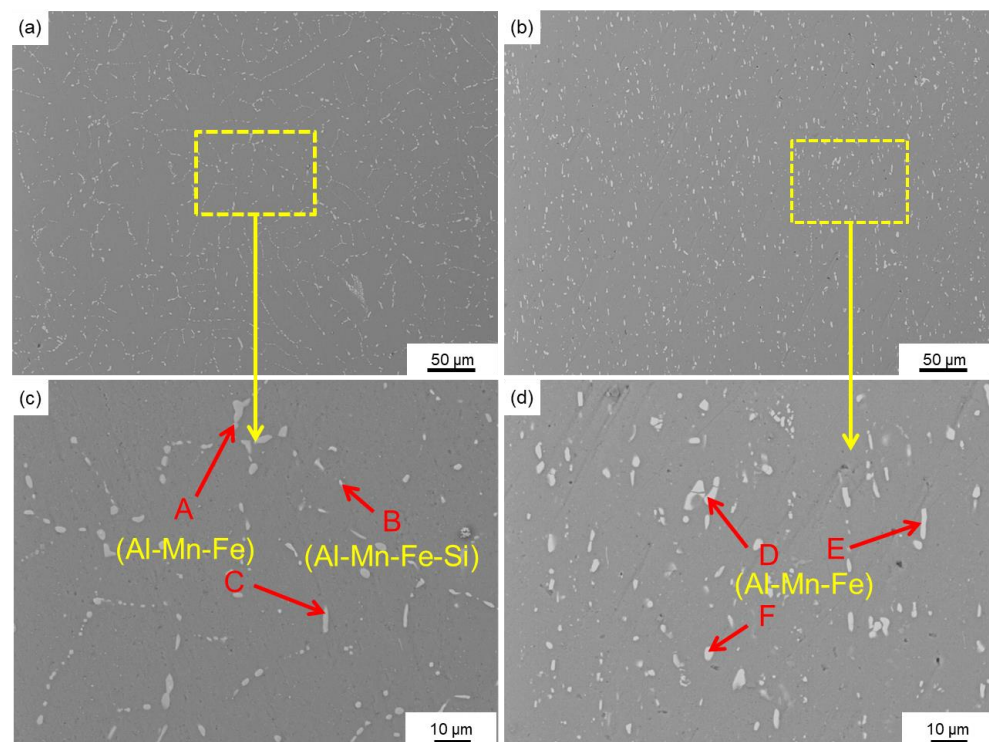
Figure 3. SEM image results of 3003 aluminum alloy under different processing states, (**a**,**c**) homogenized, (**b**,**d**) hot extruded, (**c**,**d**) are the enlarged areas of the yellow boxes in (**a**,**b**).

3.2. Surface Morphologies and Corrosion Products

The macroscopic morphology of 3003 aluminum alloy with two different processing states after acid salt spray corrosion for different times is shown in Figure 4. It can be seen that after one day of the acetic acid spray test, there were no obvious corrosion pits on the surface of the homogenized 3003 aluminum alloy, while there were many corrosion pits on the surface of the extruded 3003 aluminum alloy. As the salt spray corrosion test time was extended to 2 days, corrosion pits appeared on the surface of homogenized 3003 alloy, while corrosion pits grew larger in the extruded 3003 alloy. After the salt spray corrosion test for 4 days, the number of corrosion pits in both homogenized and extruded 3003 alloys increased significantly.
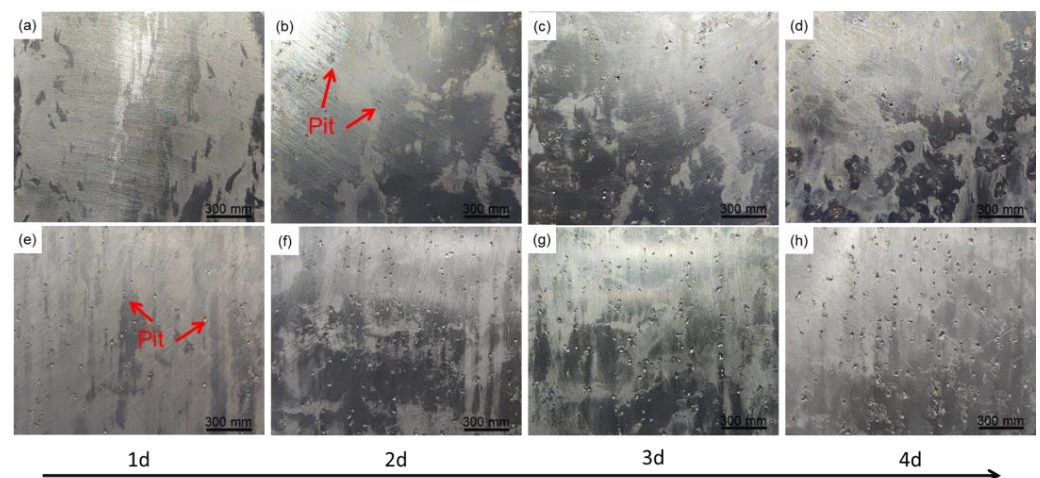
Figure 4. Macroscopic morphology of 3003 aluminum alloy in different processing conditions and different acidic salt spray corrosion times, (**a**–**d**) homogenized, (**e**–**h**) hot extruded.

The SEM images of the surface morphology of 3003 aluminum alloy under different processing states after the acid salt spray corrosion test are shown in Figure 5. After one day of salt spray corrosion, both states of the 3003 aluminum alloy exhibited corrosion pits on the surface, and the presence of corrosion products on the pits was noticeable. Over time, the size of the pits on the surface of the homogenized 3003 aluminum alloy gradually increased, and the corrosion products dropped off, with fresh aluminum alloy exposed to the corrosion solution. As shown in Figure 5f, corrosion could go underneath the surface of the material from the pitting locations. Figure 5c,e,g show that for the homogenized 3003 alloy, pitting corrosion occurred in a reticular pattern. With the increase of the salt spray corrosion time, the size of the corrosion pits grew and the number of pits increased. The corrosion products in the corrosion pits of the two different alloys were analyzed by energy spectrum, and the results are shown in Table 3. According to the results of energy spectrum analysis, it can be seen that the uncorroded areas of the 3003 alloy in two states was mainly Al_2O_3, and the corrosion product in the corrosion pit was a mixture of Al_2O_3 and $AlCl_3$.
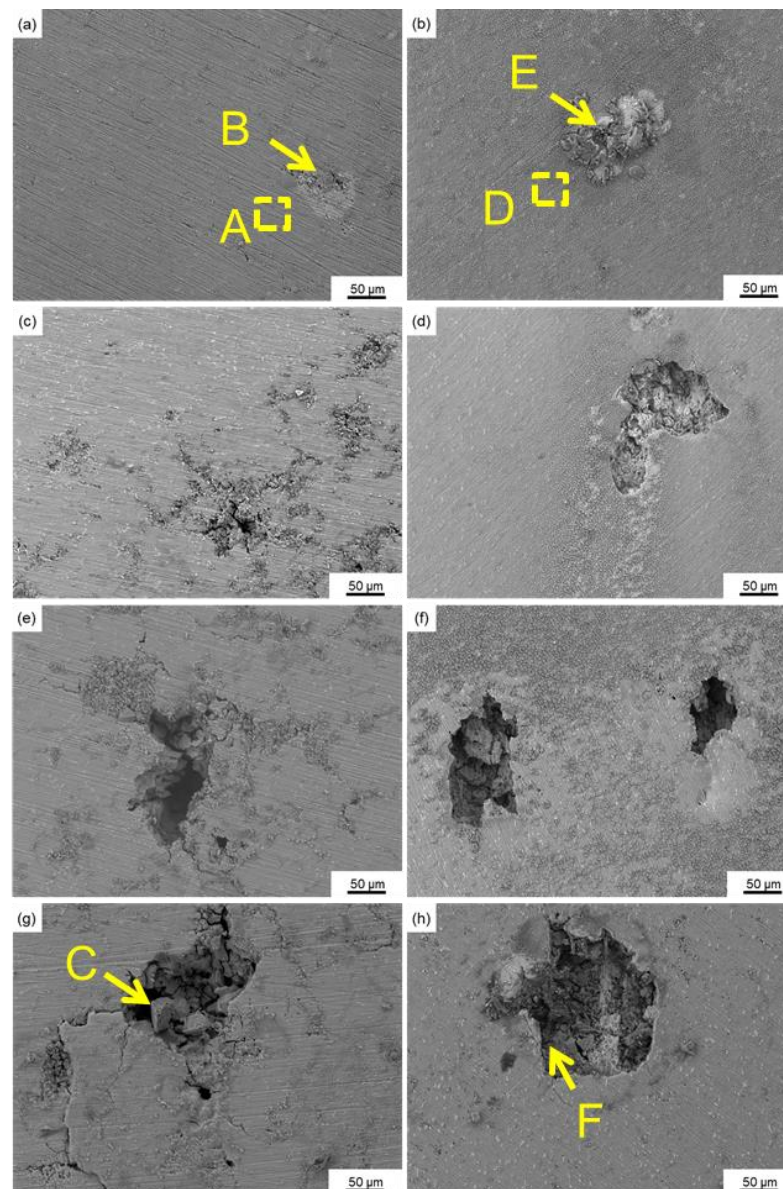
Figure 5. SEM images of 3003 aluminum alloys in different processing states with different acidic salt spray corrosion times (1,2,3,4d), (**a–g**) homogenized, (**b–h**) hot extruded.

Table 3. EDS results of the corrosion products (wt%).

Processing Status	Points	O	Al	Cl
Homogenized	A	51.95	48.05	
	B	53.33	36.59	10.08
	C	56.14	38.29	5.57
	Standard Deviation	2.14	6.18	3.19
Hot extruded	D	56.31	43.69	
	E	64.91	33.31	1.78
	F	53.85	44.25	1.91
	Standard Deviation	5.81	6.17	0.01

3.3. Density and Depth of Pitting Corrosion

After hot extrusion, the microstructure in hot extruded 3003 is significantly different from that in homogeneous 3003. The changes in grain size and orientation led to changes in grain boundary density, orientation, and residual stress. Ultimately, these surface changes may have an impact on the electrochemical behavior and hence corrosion susceptibility. Differences in the arrangement of the second phase may also have an effect on the density and extension of pitting corrosion. Figure 6 shows the localized corrosion morphology of 3003 alloy in two processing states after 4 days of acidic salt spray corrosion. Observed by laser scanning confocal microscopy, the corrosion pits of the 3003 alloy in the homogenized state were smaller in size and lower in depth compared to those in the hot extruded state. The statistical analysis method was applied to calculate the density of corrosion pits. Figure 7 shows the statistical analysis of corrosion pits, and only the diameter of pits bigger than 50 μm was counted. The pitting density of homogenized 3003 aluminum alloy gradually increased with the increase of salt spray corrosion time. After 1 day of salt spray corrosion, the pitting density of homogenized 3003 aluminum alloy was $5.67/cm^2$, while that of extruded 3003 aluminum alloy had reached $27/cm^2$. Between one day and three days of salt spray corrosion of the extruded 3003, the pitting density did not change much, and on the fourth day, the surface pitting pits increased significantly. Figure 7b shows the maximum pitting depth of 3003 alloy in the two processing conditions under different salt spray corrosion times. The pitting corrosion depth of homogenized 3003 alloy was initially as small as 20.5 μm, and gradually increased with corrosion time. The corrosion depth of hot extruded 3003 alloy reached 99.7 μm after 1 day of corrosion. After four days of corrosion, the maximum corrosion depth of homogenized 3003 was 108.9 μm, and hot extruded 3003 was 156.0 μm.

3.4. Weight Loss

Figure 8 shows the corrosion weight loss of 3003 aluminum alloy in two processing conditions under different acidic salt spray corrosion times. As the salt spray corrosion time increases, the corrosion weight loss of 3003 aluminum alloy in both states increases. The corrosion weight loss of the hot extruded 3003 aluminum alloy was higher than that of the homogenized 3003 aluminum alloy at different corrosion times, and in salt. After 4 days of fog corrosion, the corrosion weight loss in the hot extrusion state increased significantly.

3.5. Electrochemical Tests

3.5.1. Polarization Analysis

Figure 9 shows the polarization curves of the 3003 alloy with different states. The polarization curves of 3003 aluminum alloy in both homogenized and hot extruded states show the same trend, and the cathode curve extrapolation method was used to calculate I_{corr}. The cathodic reaction of 3003 aluminum alloy was mainly controlled by the reduction reaction of hydrogen ions and oxygen, while the anodic reaction was the dissolution of 3003 aluminum alloy. In addition, it can be observed from the polarization curve that there is a passivation range in both states of 3003 alloy, and their pitting potentials are close. Table 4 presents the parameters calculated through polarization curves, including

E_{corr} (corrosion potential), I_{corr} (corrosion current density), pitting potential E_{pit}, and E_{pit}-E_{corr}. Compared with the hot extruded state, the homogenized 3003 alloy had lower corrosion potential and corrosion current density, as well as a wider passivation range. The magnitude of the corrosion current density indicates the corrosion resistance of the alloy. Homogenized 3003 alloy has a lower corrosion current density, resulting in better corrosion resistance. Both states of 3003 alloy exhibit significant passivation processes. The corrosion products layer decomposes at a specific potential, characterized by pitting potential (E_{pit}), and the values of E_{pit} are shown in Table 4. When the potential reaches the passivation potential, the current growth slows down. When the potential exceeds the pitting potential, the corrosion current density sharply increases. This is because during anodic polarization, the surface of the sample reacts with the solution medium to form a corrosion product layer, which prevents further corrosion. When the potential continues to rise and reaches the pitting potential, the dissolution rate of the corrosion products layer is greater than the formation rate, and the stability is destroyed, causing the current to increase again. The pitting resistance of an alloy can also be quantified by considering the passive range, which is essentially the difference between E_{pit} and the corrosion potential (E_{corr}) [21,35]. Compared with the two states of 3003 alloy, the E_{pit}-E_{corr} value of the homogenized alloy was larger, indicating that the surface corrosion product layer of the homogenized 3003 alloy was more stable, which is a benefit to the corrosion resistance.
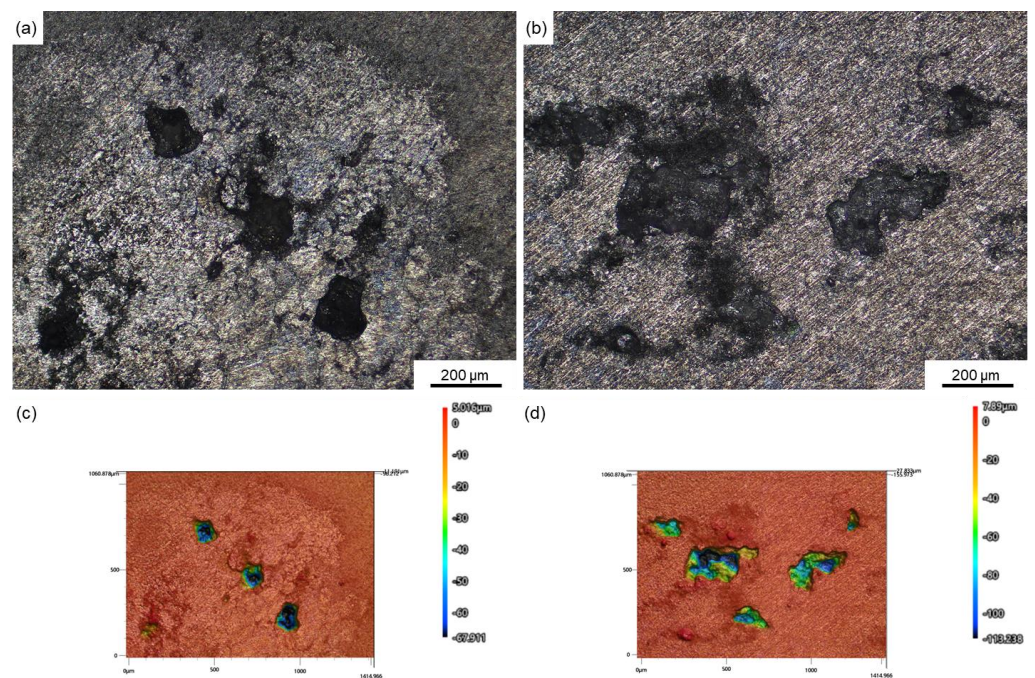

Figure 6. Typical surface morphology of 3003 alloy after 4 days of the acid salt spray corrosion test using laser scanning confocal microscopy. (**a,c**) are optical images and corresponding surface smoothness of homogenized 3003 alloy, (**b,d**) are the optical images and corresponding surface smoothness of the 3003 alloy in the hot extruded state.

**Table 4.** Electrochemical parameters derived from the polarization curves.

Specimen	E_{corr} (V_{SCE})	I_{corr} ($\mu A \cdot cm^{-2}$)	E_{pit} (V_{SCE})	E_{pit}-E_{corr} (V)
Homogenized 3003	−0.553	21.36	−0.486	0.065
Hot extruded 3003	−0.523	28.22	−0.483	0.041
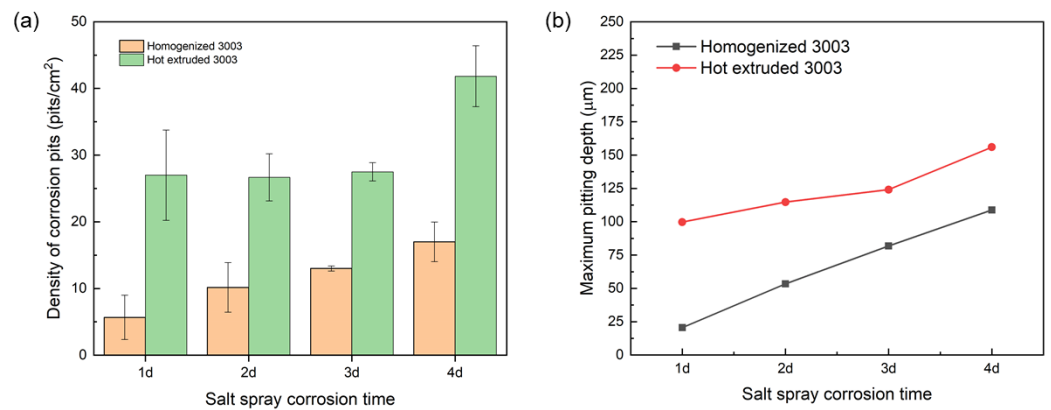
Figure 7. (**a**) Statistical analysis of corrosion pits with a diameter greater than 50 μm on the surface of 3003 alloy in two different states after the acid salt spray corrosion test, (**b**) Maximum pitting depth.
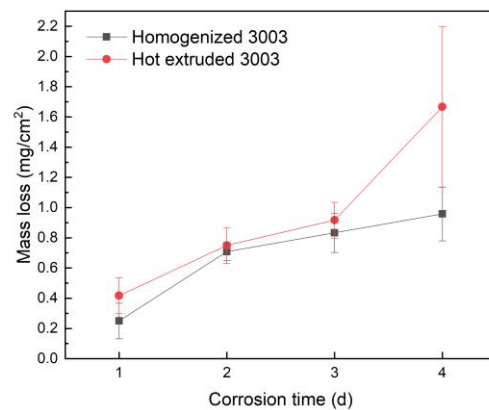
**Figure 8.** Weight loss of 3003 aluminum alloys in different processing states.
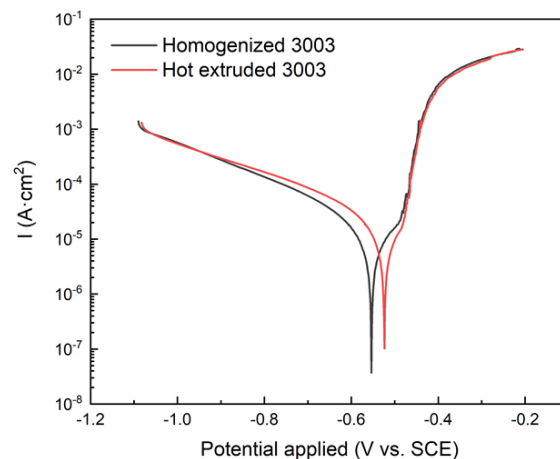
Figure 9. Polarization curves of 3003 alloy under different processing conditions in 50g/L NaCl solution.

3.5.2. Electrochemical Impedance Spectroscopy Test

Figure 10 displays the Nyquist and Bode plots for two distinct states of the 3003 aluminum alloy immersed in a 50g/L NaCl acetic acid solution, and the corresponding fitted values are presented in Table 5. Observing the Nyquist plot in Figure 10a, it becomes evident that the impedance spectra of the alloys in the two states exhibit a similar shape. In the high-frequency band, capacitance arcs resulting from activation polarization are present, while the middle-frequency band exhibits capacitance arcs associated with corrosion product layers. The observed "diffusive tail" in the low-frequency range signifies

the Warburg impedance. The generation of Warburg impedance is mainly related to the material transport on the electrode, especially the diffusion of materials in the electrolyte on the electrode surface. The initial stages of corrosion encompass the reduction of oxygen on the surface of the 3003 aluminum alloy, leading to the formation of oxides. This reduction process may generate a diffusion layer between the electrolyte and the metal surface in relation to the reactive species. The diffusion of reacting species constrains the rate of the overall reaction. In the Nyquist plot, the capacitance arc radius of the homogenized 3003 alloy is greater than that of the hot extruded alloy. The larger the radius of the capacitive reaction arc, the lower the corrosion sensitivity, indicating better corrosion resistance of the alloy.
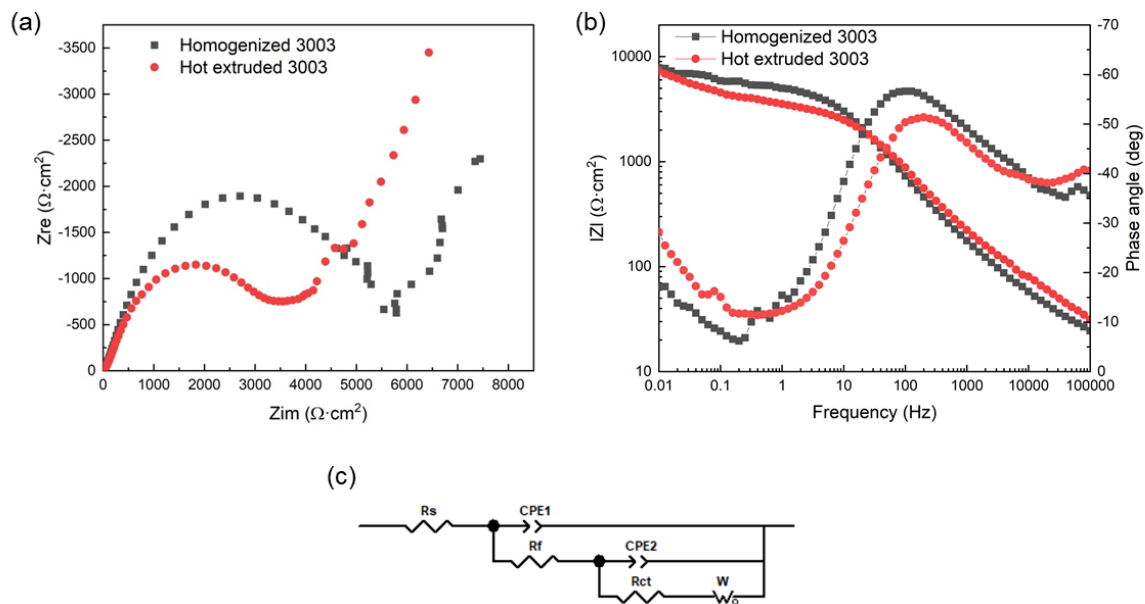
Figure 10. (**a**) Nyquist diagram, (**b**) Bode diagram, and (**c**) equivalent circuit of 3003 aluminum alloy under different processing states.

Table 5. Electrochemical parameters obtained from EIS analysis.

| Specimen	R_s $(\Omega \cdot cm^2)$	CPE_1 y0	n1	R_f $(\Omega \cdot cm^2)$	CPE_2 y0	n2	R_{ct} $(\Omega \cdot cm^2)$	W $(Ss1/2 \times 10^{-3})$	χ^2
Homogenized 3003	11.27	4.01	0.72	88.73	7.25	0.74	5415	1.28	1.93×10^{-3}
Hot extruded 3003	8.18	4.8	0.67	129.2	6.21	0.73	3407	0.88	7.33×10^{-4}

The modulus-frequency Bode plots for the tested specimens are shown in Figure 10b. In the |Z|-frequency curve of Figure 10b, the curvature in the low frequency range represents the corrosion reaction occurring at the metal/solution interface, while the radius in the medium frequency range represents the capacitance characteristics of the corrosion product layer during the corrosion reaction process. Homogenized 3003 exhibited the highest impedance at the lowest frequency of 0.01 Hz. In the high-frequency range, the impedance of the hot extruded state 3003 was higher than that of the homogenized state. According to the experimental results and related literature, the equivalent circuit is given in Figure 10c. The simulated values of the equivalent components by ZSimpWin software 3.60 are shown in Table 5. χ^2 is the precision of the simulated data, and when the value is in the order of 10^{-3} and below, it can indicate that the fitted data are in good agreement with the experimental data. The parameters Rs, Rf, and Rct in the equivalent circuit were designated as solution resistance, corrosion product layer resistance, and charge transfer resistance, respectively, while CPE_1 and CPE_2 belong to corrosion product layer capacitance and double layer capacitance, and W is Warburg diffusion coefficient [27,36]. As can be

seen from Table 5, the resistance of the corrosion product layer on the surface of the hot extruded 3003 aluminum alloy is 129.2 $\Omega \cdot cm^2$, which is higher than that of the homogenized 3003 alloy, indicating that the surface corrosion product layer of the hot extruded 3003 alloy is denser and thicker. Comparing the charge transfer resistance R_{ct} in the two states, the homogenized 3003 alloy is 5415 $\Omega \cdot cm^2$ and the hot extruded state is 3407 $\Omega \cdot cm^2$. Charge transfer resistance is often related to electrochemical reactions at the electrode surface. This resistance is mainly caused by the limitation of the rate of charge transfer between the electrode surface and the electrolyte, so the electrochemical reaction in the hot extrusion state is more active. R_p is the sum of R_f and R_{ct}. The corrosion rate of 3003 alloy in the two states was compared through R_p. The lower the R_p value, the higher the corrosion rate. Therefore, the corrosion rate of the hot extruded 3003 alloy was faster.

4. Discussion

4.1. Corrosion Mechanism

Acetic acid salt spray droplets will continuously deposit on the surface of 3003 aluminum alloy during the salt spray testing process. Since a large amount of chloride ions are dissolved in the salt spray solution, the chloride ions can migrate from the solution to the oxide film on the surface of the 3003 aluminum alloy, breaking through the dense oxide film and exposing the 3003 aluminum alloy matrix to salt spray droplets, causing alloy corrosion. In an acidic environment, the oxide film on the surface of 3003 aluminum alloy is more susceptible to damage. According to the potential–pH diagram of the Al-H$_2$O system, the oxide film starts to dissolve in acidic media with pH < 4 [37]. As the corrosion time increases, the corrosion pits tend to stabilize, and local electrochemical reactions can continue to occur in the pits. In the electrochemical process inside the pit, the aluminum matrix serves as the anode, and the intermetallic compound with a higher corrosion potential than the aluminum matrix serves as the cathode. As shown in Figure 11, SEM images of localized corrosion in the homogenized and hot extruded states are given. The starting point of corrosion is mostly near the intermetallic compounds, and the corrosion of homogenized 3003 aluminum alloy extends along the arrangement direction of the intermetallic compounds. In the hot extruded 3003 aluminum alloy, pits can also be clearly observed around the intermetallics.
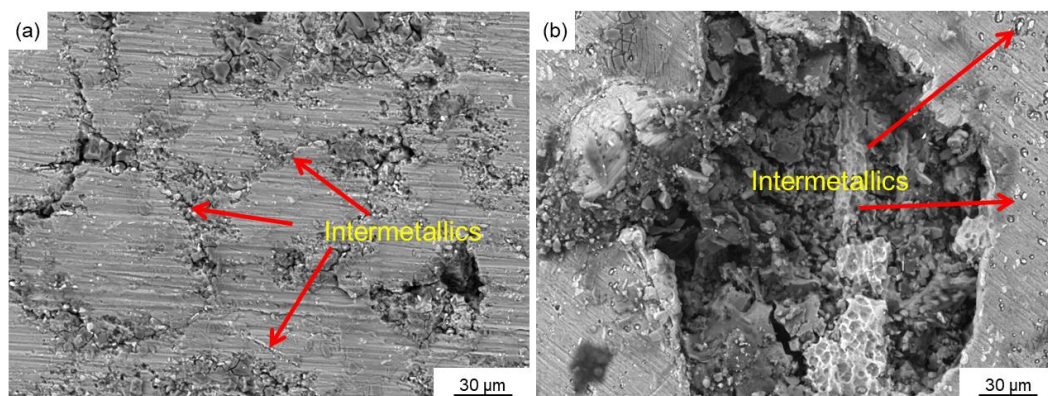
Figure 11. Surface morphology of 3003 aluminum alloy after 4d salt spray test, (**a**) homogenized 3003, (**b**) hot extruded 3003.

An oxidation reaction occurs in the anode part of the pit:

$$Al \rightarrow Al^{3+} + 3e^- \tag{1}$$

Meanwhile, the cathodic process occurs on the cathodic phase, involving the reduction of dissolved oxygen in water and the formation of hydroxide ions:

$$2H_2O + O_2 + 4e^- \rightarrow 4OH^- \tag{2}$$

Due to the use of the acidic salt spray test in this experiment, there may also be reduction of hydrogen ions during the cathodic process:

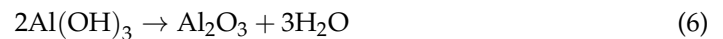$$2H^+ + 2e^- \rightarrow H_2 \uparrow \tag{3}$$

As the Al^{3+} in the pits continue to increase, in order to maintain electrical neutrality, external Cl^- will continue to migrate into the pits:

$$Al^{3+} + 3Cl^- \rightarrow AlCl_3 \tag{4}$$

$AlCl_3$ will be hydrolyzed in water to form $Al(OH)_3$:

$$Al^{3+} + 3H_2O \rightarrow Al(OH)_3 \downarrow + 3H^+ \tag{5}$$
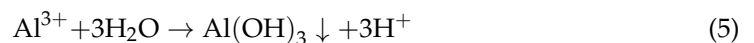
The $Al(OH)_3$ can decompose into Al_2O_3, and the reaction is as follows:

$$2Al(OH)_3 \rightarrow Al_2O_3 + 3H_2O \tag{6}$$

Therefore, the corrosion product layer on the surface of 3003 aluminum alloy under different processing conditions observed in Figure 5 is mainly Al_2O_3, and $AlCl_3$ exists in the corrosion pits.

4.2. Effect of Hot Extrusion on Corrosion Resistance of 3003 Aluminum Alloy

From Figure 4, we can observe that the number of corrosion pits on the 3003 aluminum alloy after hot extrusion is significantly higher than that in the homogenized state in an acidic salt spray environment. For 3003 aluminum alloy as a passivable metal, the following factors are generally considered to have influence on its corrosion resistance: grain size, second phase, state of surface film, etc. The grain size of 3003 aluminum alloy after homogenization treatment was large and uniform, while the hot extruded 3003 aluminum alloy had significant grain refinement due to severe plastic deformation and recrystallization. High density grain boundaries can provide formation sites for the passivation layer, while reducing the decomposition of the passivation layer [20,38]. In addition, due to plastic deformation, residual stress may exist on the surface of 3003 aluminum alloy in the hot extrusion state. Takakuwa et al. [39] believed that due to the presence of surface compressive stress, the reduction of atomic spacing will also lead to the formation of a passivation layer more rapidly. However, from Figure 5, it can be seen that during the acidic salt spray corrosion process, the pitting density of the hot extruded 3003 aluminum alloy was higher than that of the homogenized 3003 aluminum alloy. At the same time, the passivation range of the hot extruded state in the polarization curve was narrower, indicating that in the acidic salt spray environment, the corrosion resistance of the hot extruded 3003 aluminum alloy is weaker than that of the homogenized 3003 aluminum alloy. In acidic environments, the surface passivation layer of hot extruded 3003 aluminum alloy is more prone to damage, and the regeneration process of the passivation layer is also inhibited. The protective effect of the passivation layer is weakened, and chloride ions can more easily diffuse to the aluminum alloy matrix. Corrosion behavior mainly occurs on the 3003 aluminum alloy matrix. When corrosion occurs primarily through dissolution of the aluminum alloy matrix, then grain boundaries accelerate the rate of corrosion, making aluminum alloy corrosion pit expansion faster. Due to the high grain boundary density of hot extruded 3003 aluminum alloys, the rapid failure of the initial oxide film in acidic environments makes these active sites locations where corrosion rapidly occurs. Therefore,

the pitting corrosion density and maximum depth of the hot extruded 3003 aluminum alloy are higher than that of the homogenized state.

5. Conclusions

In this study, the corrosion resistance of the 3003 aluminum alloy in homogenized and hot extruded states was compared through an acid salt spray test. It is expected to help evaluate the corrosion resistance of 3003 aluminum alloy in acidic environments (such as marine engineering, chemical industry, acid rain, etc.). The corrosion behavior and mechanism of the alloys in the two states were analyzed through SEM, EDS, OM, LSCM, electrochemical testing, etc. The following conclusions can be drawn:

1. The average grain size of 3003 aluminum alloy in the homogenized state is larger, and the second phase is mainly distributed in the form of a network; after hot extrusion, the grain size of 3003 aluminum alloy is significantly reduced compared with the homogenized state, and the distribution of the second phase is more uniform, mainly along the extrusion direction.
2. In acidic salt spray environments, the corrosion resistance of the homogenized 3003 aluminum alloy is better than that of the hot extruded state, and the pitting density and weight loss of the hot extruded 3003 aluminum alloy are higher. After 4 days of acidic salt spray test, the pitting density of homogenized 3003 was about $17/cm^2$, and that of hot extruded 3003 was $42/cm^2$; the maximum corrosion depth of homogenized 3003 was 108.9 μm, and hot extruded 3003 was 156.0 μm; the homogenized state of 3003 showed a weight loss of about $0.96 \ mg/cm^2$, and hot extruded 3003 was about $1.67 \ mg/cm^2$.
3. As the acidic salt spray corrosion time increases, the corrosion of the homogenized 3003 aluminum alloy includes the increase of corrosion pit size and the formation of a reticular corrosion pit pattern, while the hot extrusion state is mainly the increase of corrosion pit size.
4. In acidic environments, the original oxide film on the surface of 3003 aluminum alloy is easily damaged, and corrosion mainly occurs in the aluminum alloy matrix. The corrosion product layer can provide a certain protective effect. The higher the grain boundary density, the higher the corrosion activity. Therefore, the hot extruded 3003 aluminum alloy has more corrosion pits and deeper pitting compared to the homogenized 3003 aluminum alloy.

Institutional Review Board Statement: Not applicable.

Informed Consent Statement: Not applicable.

Data Availability Statement: The data presented in this study are available in this article.

Conflicts of Interest: The authors declare no conflicts of interest.

References

1. Sun, Y. The use of aluminum alloys in structures: Review and outlook. *Structures* **2023**, *57*, 105290. [CrossRef]
2. Berlanga-Labari, C.; Biezma-Moraleda, M.V.; Rivero, P.J. Corrosion of Cast Aluminum Alloys: A Review. *Metals* **2020**, *10*, 1384. [CrossRef]
3. de la Fuente, D. *Corrosion of Aluminum, Aluminum Alloys, and Composites*; Elsevier: Amsterdam, The Netherlands, 2022; pp. 160–169.
4. Bajat, J.B.; Milošev, I.; Jovanović, Ž.; Jančić-Heinemann, R.M.; Dimitrijević, M.; Mišković-Stanković, V.B. Corrosion protection of aluminium pretreated by vinyltriethoxysilane in sodium chloride solution. *Corros. Sci.* **2010**, *52*, 1060–1069. [CrossRef]
5. Dursun, T.; Soutis, C. Recent developments in advanced aircraft aluminium alloys. *Mater. Des. (1980–2015)* **2014**, *56*, 862–871. [CrossRef]
6. Wei, W.; Wei, K.X.; Du, Q.B. Corrosion and tensile behaviors of ultra-fine grained Al–Mn alloy produced by accumulative roll bonding. *Mater. Sci. Eng. A* **2007**, *454–455*, 536–541. [CrossRef]
7. Hu, T.; Yin, D.; Yu, X.; Cheng, R.; Cao, H. Evolution of Microstructure in Al-Mn Alloy with a Low Ratio of Fe/Si During Homogenization. *Rare Met. Mater. Eng.* **2018**, *47*, 2631–2636.
8. Lacaze, J.; Tierce, S.; Lafont, M.C.; Thebault, Y.; Pébère, N.; Mankowski, G.; Blanc, C.; Robidou, H.; Vaumousse, D.; Daloz, D. Study of the microstructure resulting from brazed aluminium materials used in heat exchangers. *Mater. Sci. Eng. A* **2005**, *413–414*, 317–321. [CrossRef]
9. Gao, Z.; Qin, Z.; Lu, Q. Controlled Atmosphere Brazing of 3003 aluminum Alloy Using Low-Melting-Point Filler Metal Fabricated by Melt-Spinning Technology. *Materials* **2022**, *15*, 6080. [CrossRef]
10. Hong, M.-S.; Park, I.-J.; Kim, J.-G. Alloying effect of copper concentration on the localized corrosion of aluminum alloy for heat exchanger tube. *Met. Mater. Int.* **2017**, *23*, 708–714. [CrossRef]
11. Yan, P.; Zhang, Z.; Zhou, C.; Xiao, Q.; Fang, J.; Si, H.; Wang, W.; Yang, Y. Enhancement of corrosion resistance of a high Zn-yttrium aluminum alloy. *J. Alloys Compd.* **2020**, *817*, 152744. [CrossRef]
12. Cao, C.; Chen, D.; Ren, J.; Shen, J.; Meng, L.; Liu, J. Improved strength and enhanced pitting corrosion resistance of Al–Mn alloy with Zr addition. *Mater. Lett.* **2019**, *255*, 126535. [CrossRef]
13. Kim, Y.; Buchheit, R.G. A characterization of the inhibiting effect of Cu on metastable pitting in dilute Al–Cu solid solution alloys. *Electrochim. Acta* **2007**, *52*, 2437–2446. [CrossRef]
14. Xhanari, K.; Finšgar, M. Organic corrosion inhibitors for aluminum and its alloys in chloride and alkaline solutions: A review. *Arab. J. Chem.* **2019**, *12*, 4646–4663. [CrossRef]
15. Li, Q.; Xia, T.; Lan, Y.; Zhao, W.; Fan, L.; Li, P. Effect of in situ γ-Al_2O_3 particles on the microstructure of hypereutectic Al–20%Si alloy. *J. Alloys Compd.* **2013**, *577*, 232–236. [CrossRef]
16. Zykova, A.; Martyushev, N.; Skeeba, V.; Zadkov, D.; Kuzkin, A. Influence of W Addition on Microstructure and Mechanical Properties of Al–12%Si Alloys. *Materials* **2019**, *12*, 981. [CrossRef]
17. Lachowicz, M. Role of microstructure in corrosion of microchannel heat exchangers. *Inżynieria Mater.* **2018**, *1*, 4–9. [CrossRef]
18. Fontana, M.G.; Greene, N.D. A Critical Analysis of Pitting Corrosion. *Corros. Eng.* **2014**, *8*, 298–307.
19. Szklarska-Smialowska, Z. Pitting corrosion of aluminum. *Corros. Ence* **1999**, *41*, 1743–1767. [CrossRef]
20. Song, D.; Ma, A.-B.; Jiang, J.-H.; Lin, P.-H.; Yang, D.-H. Corrosion behavior of ultra-fine grained industrial pure Al fabricated by ECAP. *Trans. Nonferr. Met. Soc. China* **2009**, *19*, 1065–1070. [CrossRef]
21. Yasakau, K.A.; Zheludkevich, M.L.; Ferreira, M.G.S. Role of intermetallics in corrosion of aluminum alloys. Smart corrosion protection. *Intermet. Matrix Compos.* **2018**, 425–462. [CrossRef]
22. Liu, Y.; Cheng, Y.F. Role of second phase particles in pitting corrosion of 3003 Al alloy in NaCl solution. *Mater. Corros.* **2010**, *61*, 211–217. [CrossRef]
23. Melchers, R.E. Time Dependent Development of Aluminium Pitting Corrosion. *Adv. Mater. Sci. Eng.* **2015**, *2015*, 215712. [CrossRef]
24. Zaid, B.; Saidi, D.; Benzaid, A.; Hadji, S. Effects of pH and chloride concentration on pitting corrosion of AA6061 aluminum alloy. *Corros. Sci.* **2008**, *50*, 1841–1847.
25. Loto, R.T. Effect of SO_4^{2-} and Cl^- anionic attack on the localized corrosion resistance and morphology of 409 ferritic stainless steel. *Results Phys.* **2019**, *12*, 738–742. [CrossRef]
26. Chen, X.; Tian, W.; Li, S.; Yu, M.; Liu, J. Effect of temperature on corrosion behavior of 3003 aluminum alloy in ethylene glycol–water solution. *Chin. J. Aeronaut.* **2016**, *29*, 1142–1150. [CrossRef]
27. Liu, Y.; Meng, G.Z.; Cheng, Y.F. Electronic structure and pitting behavior of 3003 aluminum alloy passivated under various conditions. *Electrochim. Acta* **2009**, *54*, 4155–4163. [CrossRef]
28. Yin, M.; Ma, L.; Wang, J.; Ma, Y.; Ding, Y. Effect of homogenizing treatment on the corrosion resistance of 3003 aluminum alloy ingot. *Spec. Cast. Nonferr. Alloys* **2012**, *32*, 775–778.
29. Liu, Y.; Cheng, Y.F. Characterization of passivity and pitting corrosion of 3003 aluminum alloy in ethylene glycol-water solutions. *J. Appl. Electrochem.* **2011**, *41*, 151–159. [CrossRef]
30. Paredes-Dugarte, S.Y.; Hidalgo-Prada, B. Statistical Analysis of the Optical Interferometry of Pitting Process in Aluminum 3003 Sheets Exposed to Saline Environment. *Procedia Mater. Sci.* **2015**, *8*, 82–90. [CrossRef]

31. Sun, Z.; Liang, C.; Chen, Y.; Ma, Z.; Li, Q.; Yin, Z.; Ling, Y.; Xu, Y.; Liu, Z. Corrosion characteristics and prediction model of aluminum alloys in saturated Na$_2$SO$_4$ solution. *Mater. Chem. Phys.* **2023**, *308*, 128273. [CrossRef]

32. Dudina, D.V.; Kuchumova, I.D.; Batraev, I.S.; Bokhonov, B.B.; Ondar, A.A.; Grigoreva, T.F.; Shtertser, A.A. Morphological and structural changes of sintered Cu-10 wt% Al materials with different alloying levels in salt spray environment. *Mater. Lett.* **2024**, *354*, 135405. [CrossRef]

33. Usman, B.J.; Scenini, F.; Curioni, M. The effect of exposure conditions on performance evaluation of post-treated anodic oxides on an aerospace aluminium alloy: Comparison between salt spray and immersion testing. *Surf. Coat. Technol.* **2020**, *399*, 126157. [CrossRef]

34. *ASTM G85-2011*; Standard Practice for Modified Salt Spray (Fog) Testing. ASTM International: West Conshohocken, PA, USA, 2011.

35. Chen, J.; Xiao, J.; Poplawsky, J.; Michel, F.M.; Deng, C.; Cai, W. The origin of passivity in aluminum-manganese solid solutions. *Corros. Sci.* **2020**, *173*, 108749. [CrossRef]

36. Zhang, Y.; Chen, Y.; Zhang, Y.; Bian, G.; Wang, C.; Wang, A. Initial corrosion behavior and mechanism of 7B04 aluminum alloy under acid immersion and salt spray environments. *Chin. J. Aeronaut.* **2022**, *35*, 277–289. [CrossRef]

37. Graedel, T.E. Corrosion Mechanisms for Aluminum Exposed to the Atmosphere. *J. Electrochem. Soc.* **1989**, *136*, 204C–212C. [CrossRef]

38. Abdulstaar, M.; Mhaede, M.; Wagner, L.; Wollmann, M. Corrosion behaviour of Al 1050 severely deformed by rotary swaging. *Mater. Des.* **2014**, *57*, 325–329. [CrossRef]

39. Takakuwa, O.; Soyama, H. Effect of Residual Stress on the Corrosion Behavior of Austenitic Stainless Steel. *Adv. Chem. Eng. Sci.* **2015**, *5*, 62–71. [CrossRef]